Algerian Journal of Engineering and Technology

Journal homepage: https://jetjournal.org/index.php/ajet

Original Article

Sol-gel synthesis of ZnO nanoparticles for optmized photocatalytic degradation of Eriochrome Black T under UV irradiation

Auwal Yusha'u[a*], Muhammad Sulaiman Darma[a] and Kamaluddeen Abubakar Isah[b]

[a]*Department of Applied Chemistry, Faculty of Physical Science, Federal University Dutsin-Ma, P. M. B. 5001, Katsina State, Nigeria.*
[b]*Department of Chemistry, Bauchi State University, Gadau, P. M. B. 65 Gadau, Nigeria.*

ARTICLE INFO

Article history:
Received 15 January 2023
Revised 24 February 2023
Accepted 27 February 2023

Keywords:
Photocatalysis;
ZnO;
Box-benhken;
UV-light;
Eriochrome Black T.

ABSTRACT

In this work, zinc oxide (ZnO) nanoparticles was synthesized by sol-gel method and characterized using x-ray diffraction (XRD), scanning electron microscopy (SEM), Fourier transform infrared (FT-IR), energy dispersive spectroscopy (EDS) and ultraviolet-visible (UV-Vis) spectrophotometry. The XRD analysis of the as synthesized catalyst revealed a hexagonal wurtzite structure. The average particle size and band gap values were 24.67nm and 3.28eV respectively. The peak observed at 452cm^{-1} corresponds to Zn-O stretching vibrational band. The effect of operating paramers such as initial concentration of eriochrome black-T (EBT), concentration of catalyst and pH of the solution was optimized using box-benhken design (BBD) and response surface methodology (RSM). The optimum photodegradation efficiency of 96.59% was obtained at 15.00mgL^{-1}of EBT concentration, 0.40gL^{-1} catalyst concentration and initial pH of 9.00. The degradation model was statistically remarkable with $p < 0.0001$% in which the EBT initial concentration and catalyst concentration were the most significant variables influencing the degradation of EBT over ZnO photocatalyst under UV irradiation.

1. Introduction

The occurrence of azo-organic dyes in the aquatic environment has many potential negative effects on human health [1]. Currently, about 60-70% of all the dyes in paint, ceramic, paper, rubber, plastic, leather and pharmaceutical industry are azo-dyes [2]. Many of these industries have been challenged significantly over the discharged of azo dyes into the aqueous ecosystem. Eriochrome black-T (EBT) is a molecule with one azo bridge linking substituted aromatic structure [3]. It is widely used in textiles, research, teaching laboratories to determine water hardness and for biological staining [4]. On the other hand EBT presently classified as hazardous pollutant due to its chemical stability, non-biodegradable and high solubility in water. Some of the adverse effects of EBT includes, difficulty in breathing, vomiting, diarhoa, and skin and eye irritation [5]. However, EBT is difficult to remove from the aquatic environment due to its large molecular structure. The removal of EBT by adsorption, coagulation, flocculation and biodegradation are ineffective [6] and all of these methods are considered to be laborious, costly and requires extra planning to remove the biproducts [7]. Owing to the complex properties of EBT, there is no specific treatment available to ensure its complete removal thus far. Therefore, development of reliable process that could effectively eliminate the EBT from water is essential for safeguarding human health.

Nowadays, heterogeneous photocatalysis represents an efficient and effective technology for the removal of

* *Corresponding author*. Tel.: +2349026265322
E-mail address: auwalyushau2018@gmail.com
Peer review under responsibility of University of El Oued.
 DOI: https://doi.org/10.57056/ajet.v8i1.100

organic pollutants from the environment [8]. This method however, highlighted a beautiful success in effective degradation of dyes due to their ability for total oxidation compared with the classical and conventional methods for the treatment of wastewater effluents [9]. The process involves the use of holes and hydroxyl radicals harvested from the sufficiently light –excited photoresponsive catalyst [10]. Different photoresponsive catalysts such as TiO_2, ZnO, WO_3, ZrO_2, Fe_2O_3, SnO_2, $SiTiO_2$ and V_2O_5 were reported as a potential photoresponsive catalysts [11]. Zinc oxide (ZnO) now considered as a promising photocatalyst since it demonstrates high photocatalytic efficiencies for the removal of organic pollutants in comparison to other metal oxides due to its chemical stability, non-toxic, low cost, large excitation energy (60meV) and environmental friendly species [12, 13, 14]. In addition, surface area and surface defects of zinc oxide (ZnO) are important factors to enhance the photocatalytic activity [15]. The higher the effective surface area lead to higher adsorption of organic molecules, while enhanced photocatalytic activities, lead to its efficient degradation. Though ZnO photocatalyst has been synthesized by several techniques such as hydrothermal, sol-gel, chemical vapour deposition (CVD), mechanochemical, microemulsion, electroplating, atomic layer decomposition, sputtering and anodic oxidation method [16]. But sol-gel synthesis, is preferred for many applications since it is a high purity, high homogeneity, controlled porosity combined with the ability to form large specific surface area at low temperature [17]

However, the photocatalytic performance of ZnO nanoparticles have been evaluated with different organic and inorganic pollutants [18]. Maureen *et al* [19] reported the photocatalytic degradation of a basic dye using ZnO nanocatalyst and the results demonstrated the significant response, 95.48% at 150 mins. Kian *et al* [20] studied the photocatalytic decolourization and mineralization of reactive azo dye, eriochrome black-t using commercial ZnO photocatalyst under UV irradiation. The results revealed that 83% of EBT decomposed under 96W of UV irradiation for 20 mins. Similarly, Chen *et al* [21] investigated the photocatalytic degradation of azo dyes over ZnO photocatalyst and the results showed that the removal of azo dyes increases with increasing of the catalyst dosage and decreases with increasing of the initial concentration of azo dyes and the acidic condition is favourable for degradation. However, in the previous EBT photocatalytic degradation studied, especially the works of Kian *et al* [20] reported the optimization of operational parameters over the commercial (without synthesis and characterization) ZnO nanoparticles using a central composite design (CCD) of the response surface methodology (RSM) while Wang *et al* [4] studied the photocatalytic degradation of EBT over the synthesized and characterized ZnO nanoparticles but the effect of the primary parameters was not optmized by either CCD, FCCD or BBD of the RSM.

Despite the coexisting works in the literature, herein we aim to report the sol-gel synthesis of ZnO nanoparticles using zinc nitrate as precursor, characterize by XRD, SEM, FT-IR, EDS and UV-Visible spectrophotometry and evaluated it's photocatlytic activity using eriochrome black t (EBT) as a model substrate. The reaction variables such as initial concentration of EBT, concentration of catalyst and initial pH was optimized using box benhken design (BBD) of response surface methodology (RSM). Similarly, the role of reactive radicals (h^+, •OH and $•O^-_2$) generated during the photocatalytic removal of EBT over the ZnO nanoparticles also was investigated.

2. Materials and Methods

2.1. Material

Zinc nitrate dihydrate ($Zn(NO_3)_2.2H_2O$, 97%), nitric acid (HNO_3, 98%) oxalic acid dihydrate and Eriochrome Black T ($C_{20}H_{12}N_3O_9S$, 98%) were supplied by Sigma Aldrich, Canada, while sodium hydroxide (NaOH, 98%) and ammonium hydroxide (NH_4OH, 98%) were obtained from BDH, Poole, England. All chemicals were used as received from the manufacturers without further purification. The structural formula of EBT is shown in Fig. 1.

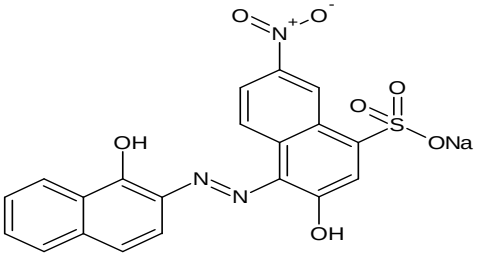

Fig 1. Molecular structure of EBT.

2.2. ZnO Synthesis

The nanoparticle ZnO was synthesized by a sol-gel method previously described by Chen *et al* [21]. The procedure was adopted and modified for the present ZnO synthesis. Specifically, 2.45g of zinc nitrate was dissolved in 60mL of deionized water and stirred vigorously at 60℃ for 30 min to obtain solution X. Solution Y was prepared by dissolving 2.78g of oxalic acid dihydrate in 80mL and stirred at 50℃ for 30 min. Then solution Y was added to the warm solution X drop wise and continuously stirred at

pH 8 for 1 h. A white sol was obtained and aged to form a gel which was dried at 80°C for 24 h. Finally, ZnO was calcined in a muffle furnace at 450°C for 4 h, and cooled to room temperature. The resultant sample was levelled as a ZnO nanoparticles.

2.3. Characterization methods

The as synthesized photocatalyst was analysed using diffractograms from Philips X pert Pro diffractometer operated with a CuK_{α} radiation (λ= 1.54468 Å) in the 2θ range 5-70 ° at 30 kV, 30 mA and scanning rate of 2 min.. The lattice parameters such as spacing distance between the adjacent planes in the miller indices d_{hkl}, lattice constant a, b and c, (Eq.1-4). The calculated values for the synthesized catalyst was compared to the unit cell parameters for the standard ZnO (JCPDS 070-7085)

$$a = b = \frac{\lambda}{\sqrt{3}\sin\theta_{100}} \quad (1)$$

$$c = \frac{\lambda}{\sin\theta_{001}} \quad (2)$$

Where a, b, and c are the lattice constants, λ is the wavelength of x-ray radiation (1.5406 Å), θ is Bragg's angle. The average crystalline size has been estimated using Debye-Scherer (eq. 3) and surface area for ZnO nanoparticle was calculated from the eq. (6-8), respectively.

$$D = \frac{k\,\lambda}{\beta\,\cos\,\theta} \quad (3)$$

$$SSA = \frac{6000}{D\times\rho} \quad (4)$$

Where D is the average particle size, k is the Debye-Scherer constant (0.89), λ is the wavelength of the x-ray radiation, β is the full width at half maximum intensity (FWHM), θ is the diffraction angle at the position of peak maximum, SSA is the specific surface area, SA is the surface area, ρ is the density of ZnO (5.69 gcm^{-3})

The surface morphology of the synthesized photocatalysts was recorded on LEICA Stereo scan-440 interfaced with Phoenix proxy energy dispersive x-ray spectrometer. The facility was operated at the same scale (30 µm), magnification (2,500) and accelerating voltage (15 kV). The FTIR spectra of the catalysts were recorded using Agilent Cary 630 diamond total attenuated reflectance Fourier transform infrared spectrometer (ATR-FTIR).

2.4. Surface Area of the Photocatalyst

The surface area (S.A) of the synthesized photocatalyst was determined from the x-ray diffraction (XRD) raw data. The S.A for the bare ZnO photocatalyst has been estimated using equation 5 and 6 respectively.

$$SSA = \frac{S.A}{V\times\rho} \quad (5)$$

$$S.A = SSA \times V \times \rho \quad (6)$$

Where SSA is the specific surface area, SA is the surface area, ρ is the density of ZnO (5.65gcm^{-3}).

2.5. Band gap determination

The band gap energy (E_g) values for the ZnO photocatalyst was obtained from the electronic data recorded over the wavelength range 200-800 nm on the Lambda 35 Perkin Elmer UV-Visible spectrophotometer. However, E_g values for the synthesized catalyst was calculated using the Schuster-Kubelka-Munk relation (Eq. 7) [22].

$$(\alpha\, h\, \nu)^{\frac{1}{n}} = K\left(h\nu - E_g\right) \quad (7)$$

Where α is the absorption coefficient obtained from Beer's law, h is the Planck's constant, *ν* is the frequency of vibration, K is a proportionality constant and E_g is the band gap energy of the semiconductor photocatalyst. The E_g values were calculated from the intercept of the plot of $(\alpha\, h\, \nu)^{\frac{1}{n}}$ against h**ν**. If scattering is insignificant the term $\alpha\, h\, \nu$ is proportional to a function of reflectance $[F(R)(\alpha\, h\, \nu)]$. Since the semiconductor ZnO used in this experiment is a direct band gap allowed sample transition and thus the denominator of the exponent n = ½.

2.6. Photoexperiments

A batch experiment was conducted in an immersion well photoreactor shown in Fig. 2, which was made up of a 7 cm diameter, 30 cm long cylindrical quartz glass housed in a 1 L round bottom flask having an effective volume of 0.6 L. The UV light source is a 90 W lamp emitting light at 400 nm. Samples were collected through a sample port.

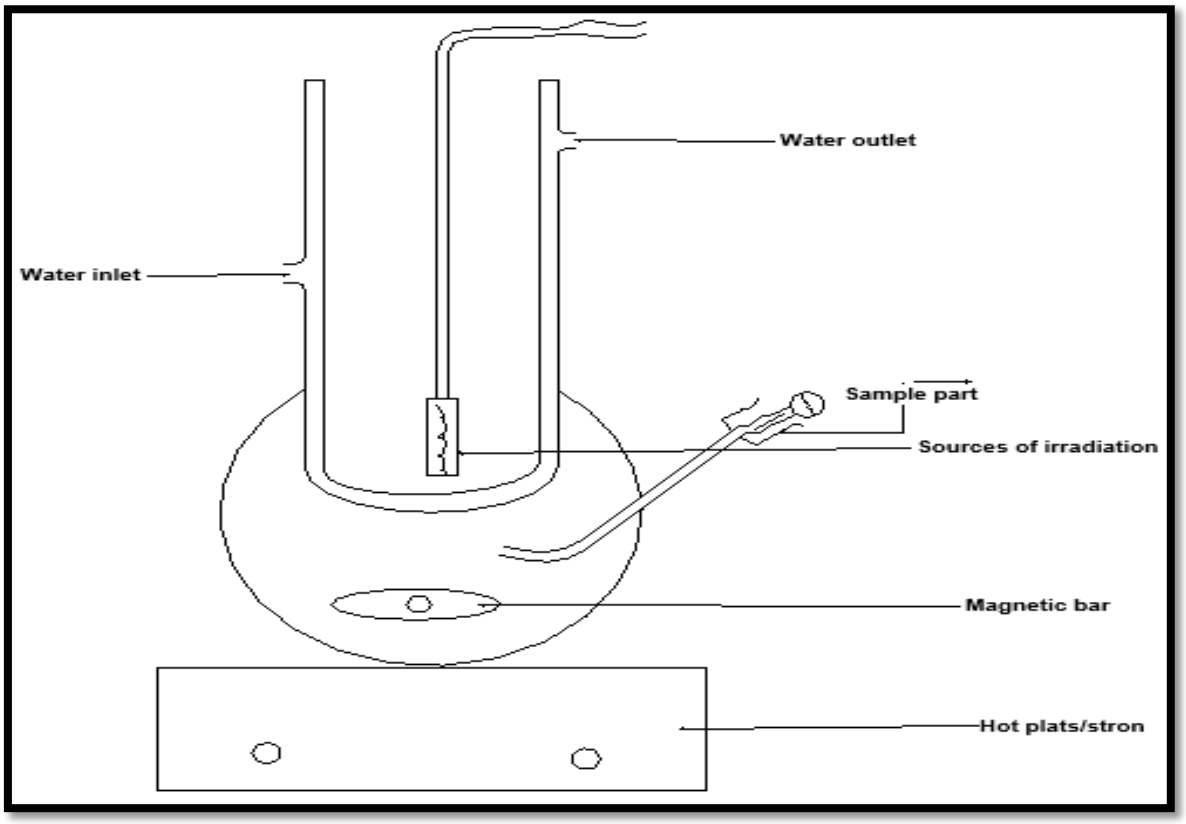

Fig 2. Immersion well photoreactor [22]

Exactly 400 ml aqueous solution of the desired amount of EBT and ZnO photocatalyst were added to the photoreactor and the pH of the suspension was adjusted using 0.5 molL^{-1} NaOH and H_2SO_4. This mixture was exposed to irradiation under continuous stirring at room temperature (25 °C) for 180 min. After every 20 min, an aliquot was filtered using 0.45 µm cellulose nitrate filter and analysed for residual concentration of EBT at 564.38 nm using a Lambda 35 Perkin Elmer UV-Vis spectrophotometer. The percent photodegradation efficiency (% D) was calculated using Eq. (8).

$$D\% = \frac{[EBT]_0 - [EBT]_t}{[EBT]_0} \times 100 \quad (8)$$

Where $[EBT]_o$ and $[EBT]_t$ are the initial and final concentration of Eriochrome Black T, and t is the irradiation time.

2. 7. Box-benhken experimental design

The experimental design and statistical analysis was done using the Box-Benhken design of Response Surface Methodology (RSM) due to its uniqueness in generating a higher-order surface response. An experimental design was carried out at three-level-three-variable box benhken design (BBD). These independent variables are the initial EBT concentration (X), catalyst loading (Y) and initial pH (Z) operated at three levels (low, central, high) coded -1, 0 and +1 (Table 1). Other variables such as agitation speed, light intensity, oxygen pressure and delivery volume were maintained constant. A total of 17 experiments (N) were performed based on the formula $N = 2^n + 2n + 3$. Where n is the number of variables. The % D obtained from these experiments were processed using Design Expert software DX 13.0 upgraded version to obtain the predicted responses, response surface and regression model for the EBT degradation.

Table 1**.** The level factorial box-benhken design (BBD)

Variable	**Notat**	**Levels (Codes)**		
EBT(mg/L)	X	(-1)10.00	(0)15.00	(+1)25.00
Cataly (g/L)	Y	(-1)0.10	(0) 0.40	(+1)0.80
Initial pH	Z	(-1)3.00	(0) 9.00	(+1)12.00

2.8. Controexperiments

To evaluate the photocatlaytic removal of eriochrome black-t over ZnO nanoparticle, two control experiments

(adsorption and photolysis) were conducted under two different experimental conditions. For the adsorption experiment, desired amount (0.1g) of the photocatalyst (ZnO) was mixed with 400mL aqueous solution of the desired amount (10mg/L) of EBT in a photoreactor and magnetically stirred for 180 min throughout in the dark. Thereafter, every 20 mins samples were taken for the analysis after separating the photocatalyst particles using a Lambda 35 Perkin Elmer UV-Vis spectrophotometer at a wavelength of 564.38 nm. For the photolysis experiment, 400mL aqueous solution of the desired amount (10mg/L) of EBT without the photocatalyst was exposed to 90W UV lamp at room temperature. After every 20 mins, the samples were taken for analysis using a Lambda 35 Perkin Elmer UV-Vis spectrophotometer at a wavelength of 564.38 nm. The photodegradation efficiency of EBT via adsorption and photolysis was calculated using Eq. 8. These were compared with photocatalysis over ZnO photocatalyst.

2.9. Radiscavenger experiments

In order to determine the major role of reactive radicals generated during the photocatalytic removal of EBT over ZnO nanoparticle, the main reactive radicals and holes were detected through radical scavenging experiments. During the photocatalytic process, the holes (h^+), hydroxyl radical (•OH) and superoxide radical ($•O^-_2$) are trapped by adding ammonium oxalate (AO), (h^+ scavenger), *t*-butanol (•OH scavenger), and *p*-benzoquinone ($•O^-_2$ scavenger) into the reaction solution respectively. Typically, 10mg of ZnO and 10mM of radical scavengers were introduced into 15mg/Lof EBT solution, then the suspension was irradiated using the 96W of UV irradiation for the same time. Finally the EBT photodegradation efficiencies were calculated using Eq. 8.

3. Results and Discussion

3.1. Catalyst Characterization

3.1.1. XRD Analysis

The x-ray diffraction (XRD) is an excellent technique used to determine the microstructures, crystal phase, purity, lattice parameters, specific surface area and crystallinity of the synthesized ZnO nanoparticles. The XRD patterns of the as-synthesized ZnO catalyst is shown in Fig 3.

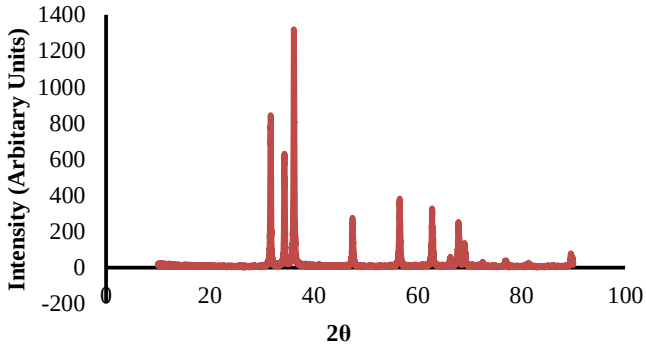

Fig.3: X-ray diffraction of ZnO nanoparticles

It is clear that the Bragg reflections at 2θ values of 31.8^0,34.4^0, 36.3^0, 47.6^0, 56.7^0, 62.9^0, 66.5^0, 68.0^0 and 69.1^0correspond to the structural miller indices (100),(002), (101), (102), (110), (103), (200), (112),and (201) of ZnO crystal plane respectively. All peaks in the diffraction patterns for the synthesized ZnO photocatalyst were matched to the standard hexagonal wurtzite structure of ZnO [23] (JCPDS 01-070-8072) [24]. The unit cell parameters for the synthesized photocatalyst were calculated based on ZnO lattice plane 100 and 002. It would be seen that the values obtained (Table 2) agree with the standard lattice parameters (a=3.2465Å and c=5.2030Å; JC PDS Card no; 070-8072) of ZnO nanoparticles. This confirmed that the prepared ZnO photocatalyst was maintained the hexagonal wurtzite structure of the standard ZnO photocatalyst.

Furthermore, no additional peaks related to impurities were detected by the diffractometer. This clearly indicated that the single phase and high purity of the synthesized photocatalyst [25]. However, Table 2 showed that, the crystallite size (24.67nm) was smaller than the specific surface area ($36.87 m^2g^{-1}$) of as-synthesized ZnO photocatalyst.

Table 2. Lattice parameters, crystallite size and specific surface area and band gap of the synthesized ZnO photocatalyst

Catalyst	Lattice parameters (Å)	Size (nm)	Surface Area (m^2g^{-1})	Band gap (eV)
ZnO	a = b = 3.247 c = 5.2031	24.67	36.87	3.28

The higher specific surface area may be attributed to its smaller particles size, and thus, should facilitate faster reaction between ZnO catalyst and the reaction medium which mainly occurs at the interface and strongly on the specific surface area of the catalyst [11].

3.1.2. SEM Analysis

The scanning electron microscopy (SEM) image beautifully demonstrated the existence of prepared ZnO nanoparticles. The nanoparticles were spherical, oval in shape and aggregated porous powder like morphology and individual particles were also observed. The surface morphology of the as-synthesized ZnO nanoparticles is displayed in Fig. 4.

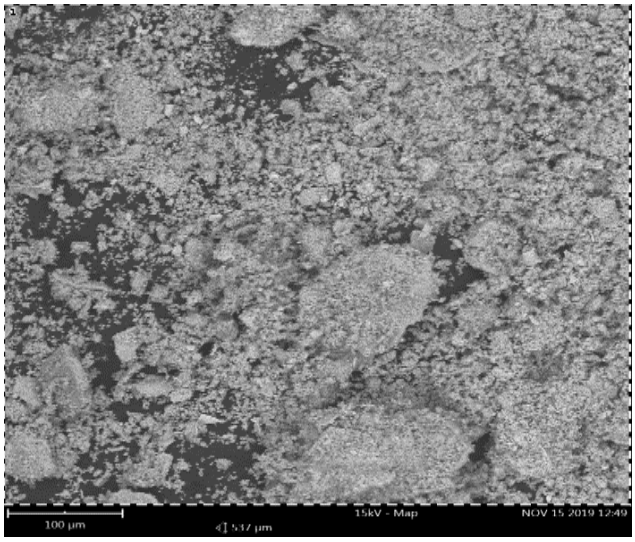

Fig 4.The SEM image of ZnO nanoparticles

From the figure, aggregation of particles is seen in the ZnO photocatalyst. The agglomeration could be attributed to the densification resulting of narrow space among the particle [26, 27]. The SEM image also revealed mostly particles of ZnO nanoparticles in small size but some particles appeared with higher particles size also. This supports the results of M. F. Lanjwani *et al*. [28] for the photocatalytic degradation of eriochrome black t dye by ZnO nanoparticles using multivariate factorial, kinetics and isotherm model.

3.1.3 EDS Analysis

The energy dispersive spectroscopy (EDS) is a powerful technique used for the find out the elemental composition of the nanoparticles or any other materials [29]. The EDS of the synthesized ZnO nanoparticles is presented in Fig. 5.

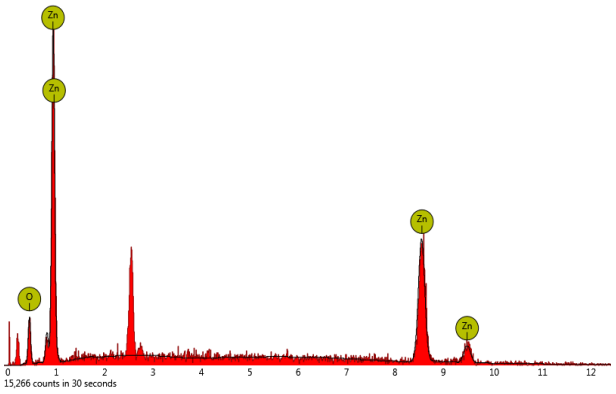

Fig 5. EDS spectrum of ZnO Nanoparticles

The EDS of the prepared ZnO (Fig. 5) was examined and the assigned peaks were for Zn and O, without any cotamination peaks. The percentage weight (Table 3) of Zn and O were 96.50 % and 3.50% respectively. The results confirm that the synthesized ZnO nanoparticles were was pure and no other element present in the synthesized photocatalyst. This however, supports the results reported in the literature[29, 30].

Table 3. Elemental composition of the synthesized ZnO Nanoparticles

Atomic number	Symbol	Name	Atomic Conc (%)	Weight Conc (%)
30	Zn	Zinc	88.11	96.50
8	O	Oxygen	11.89	3.50
Total			**100**	**100**

3.1.4. FT-IR Analysis

The Fourier Transform Infrared (FT-IR) spectroscopy is a great technique used for the characterization and identification of materials and compounds by examine their unique modes of vibration [28]. The FT-IR spectra of the as synthesized ZnO nanoparticles is shown in Fig. 6

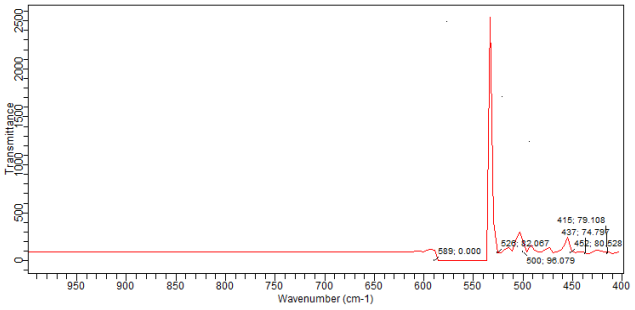

Fig 6. FT-IR spectra of the ZnO photoctalyst

Fig 6. shows a number of peaks due to the reagents used for preparation of ZnO nanoparticles. The absorption band at 80cm^{-1}, 96cm^{-1}, 79cm^{-1}, 82cm^{-1}, 797cm^{-1}, 108cm^{-1}, 96cm^{-1} and 74cm^{-1} in the sample was due to the residual carboxylate anions which might remain adsorbed on the surface of ZnO nanoparticles. The IR absorption band observed at 415cm^{-1}, 437cm^{-1}, 452cm^{-1}, 500cm^{-1}, 526cm^{-1}, 528cm^{-1} and 589cm^{-1} in the sample was corresponds to Zn-O stretching vibration. This confirm the present of pure ZnO nanoparticles which be proved for the literature value of the IR spectra having the range 680-300cm^{-1} for ZnO [29, 31].

3.1.5. Band gap measurement

The band gap energy for the obtained ZnO photocatalysts were calculated from the absorption data using Kubelka-Munk's intercept of the plot of $(\alpha h\upsilon)^2$ against hv as displayed by Fig. 7. This plot is linear in the vicinity of the band gap region for the ZnO nanoparticles. The band gap energy values for the ZnO photocatalysts was 3.28 eV, confirming the ability of the ZnO to absorb UV-light.

.

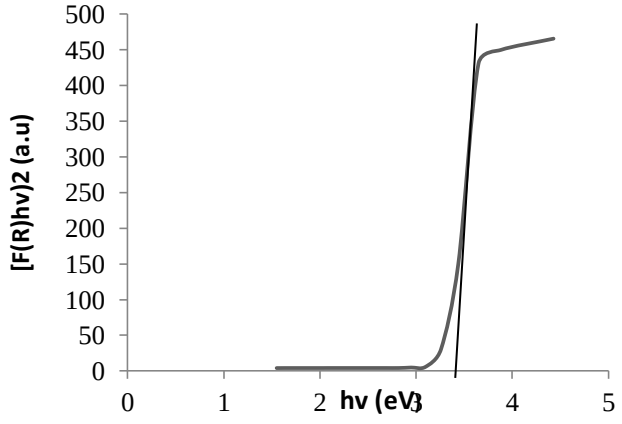

Fig 7. Tauc's Plot for the ZnO nanoparticles

3.2 Preliminary investigation

3.2.1. Initial Concentration

To determine the effect of initialoncentration of EBT an Experiment was conducted by varying initial concentration of EBT (5-25mg/L). While the amount of the photocatalyst (0.5g/L), initial pH (8) of the suspension, volume of the solution and illumination time were kept constant and the results obtained was depicted in Fig. 8

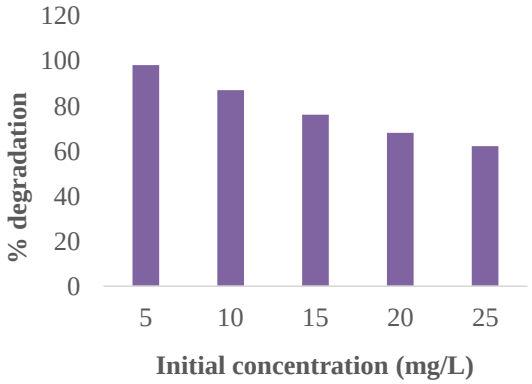

Fig 8. Effect of initial concentration of eriochrome black t

It was seen from the Fig. 8 that the percentage degradation efficiency increases with decreasing of initial concentration of the EBT. This is because the number of photons absorption by the catalyst increases in the lower concentration regime. This suggest that as the initial concentration of EBT increases the requirement of the photocatalyst surface needed for the degradation also increases. Since the illumination time and amount of the photocatalyst are constant, the •OH radical (primary oxidant) formed on the surface of ZnO is also constant. Consequently, the relative number of the free radical attacking the EBT molecule decreases with increasing amount of the photocatalyst. While the percentage photodegradation of EBT decreases with increasing of initial concentration. This is because the number of photons absorption by the photocatalyst decreases in the higher concentration of EBT and requirement of the catalyst surface required for the degradation also increases.

3.2.2. Catalyst concentration

To determine the optimum amount of catalyst loading on the photocatalytic degradation of EBT, various amount of catalyst (0.01-0.06g/L) were used while initial concentration (10mg/L), initial pH (8), volume of solution and illumination time were kept constant. Fig. 9, shows the effect of catalyst loading for the photocatalytic degradation of EBT over ZnO nanoparticles. From the Fig. 9, it can be seen that the increase in the amount of ZnO from 0.01 to 0.02g /L slightly increases the percentage degradation of EBT due to availability of active sites with increases of catalyst loading.

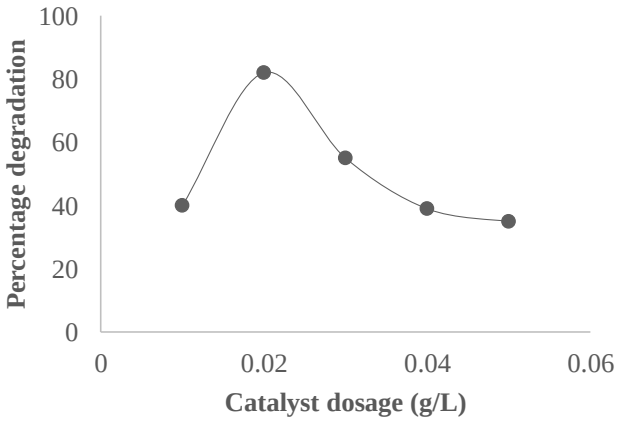

Fig 9. Effect of catalyst concentration

Decline in the degradation efficiency of EBT was observed at amount of catalyst above 0.02g/L. Thus 0.02g/L of ZnO photocatalyst was found to be the optimal amount when compared with the rest amount of catalyst. The slight decrease in degradation of EBT may be due to the aggregation of ZnO nanoparticle.

3.2.3. Initial pH

To investigate the effect of initial pH on the photocatalytic degradation of EBT over ZnO photocatalyst, an experiment was performed by varying the initial pH in the range (2-12). In the experiments pH was adjusted by adding appropriate drop of H_2SO_4 or KOH solution while the initial concentration, catalyst dosage, volume of solution and illumination time were kept constant and the result was displayed in Fig. 10. From the figure it can be seen that there was a mild increase in degradation with an increase in initial pH.

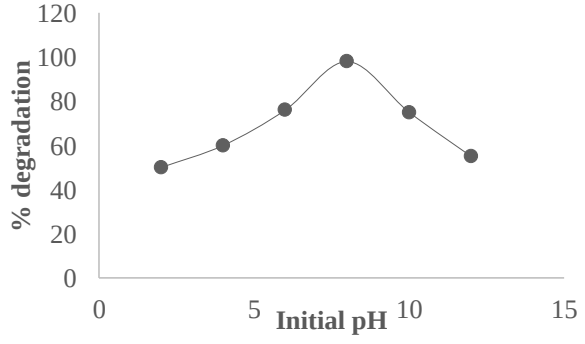

Fig 10. Effect of initial pH

It is also observed that the percentage removal is higher at initial pH value greater than 2 and less than 10. The solution pH affects the surface charge of ZnO and availability of hydroxyl radicals. At high pH values (greater than 8) the hydroxyl radicals are so rapidly scavenged that they do not have the opportunity to react with EBT. The pH affects not only the surface properties of ZnO, but also the dissociation of EBT and formation of hydroxyl radicals. Thus, the degradation of EBT in this work was more efficient under basic (8) conditions than under acidic conditions. This is because under basic conditions, the •OH radicals are generated more easily by oxidizing more hydroxide ions available on catalyst surface, the efficiency of the process is enhanced. Similarly, at low pH, reduction by electrons in the conducting band may play a very important role in the degradation of EBT due to the reductive cleavage of azo bonds.

3.3. Photoevaluation

In order to investiagate the photocatalytic activity of the as synthesized ZnO nanoparticle for the removal of eriochrome black t, three experiments were performed at different conditions and the result was depicted in Fig 11. The Fig 11 shows that the percentage removal of EBT obtained, 10.11% under photolysis is not significant after 180 mins. This shows that UV light has little effect on the removal of EBT from the aqueous environment.

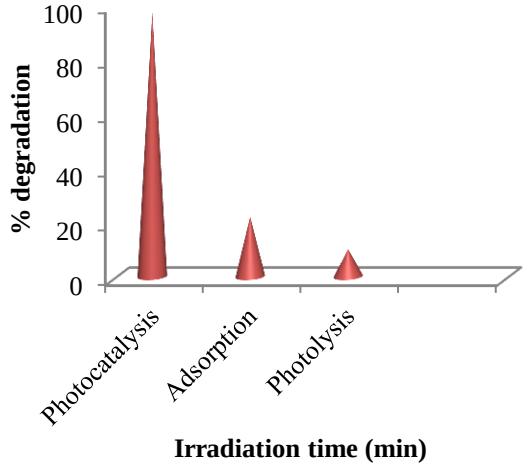

Fig 11. Effect of irradiation time on the photolysis, adsorption and photocatalysis of EBT over prepared ZnO nanoparticle.

The percentage removal of EBT resulted under adsorption was 20.87%. While the photoefficiency for the removal of EBT using the synthesized ZnO photocatalyst under ultraviolet light after 180 mins was 96.14%. This demonstrated that light and catalyst play an important roles in heterogenous photocatalysis.

3.4. Recyclability of ZnO Nanoparticles

To investigate the stability and reusability of the as synthesized ZnO nanoparticles, an experiment was carried out at the optimum conditions of the photocatalytic degradation of eriochrome black t using the prepared ZnO. Residual catalyst from removal experiment was filtered, washed and dried and then recycled in fresh experiment and the result was presented in Fig. 12.

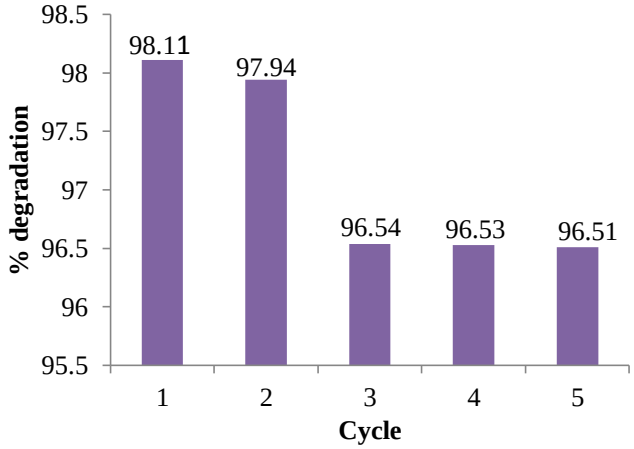

Fig 12. Recylability of ZnO nanoparticles in degradation of EBT.

Fig.12 shows that the removal of EBT decreased steadily from the 1st and 2nd cycles but 3rd, 4th and 5th cycles remained almost the same. This demonstrates the durability, stability and effectiveness of the prepared ZnO photocatalyst in the removal of eriochrome black t from the aqueous environment.

3.5. Mechanism of EBT Photodegradation over ZnO Nanoparticles

The mechanism of the photocatalytic degradation process generally involves the photoexcitation, separation, migration of charge and redox reactions on the surface of the photocatalyst [32]. The reactive species generated during illumination of photocatalysts are hole (h^+), hydroxyl radical (•OH) and superoxide ($•O_2$). A mechanism for photocatalytic removal of eriochrome black t on the ZnO nanoparticle under UV irradiation is shown in Fig. 13.

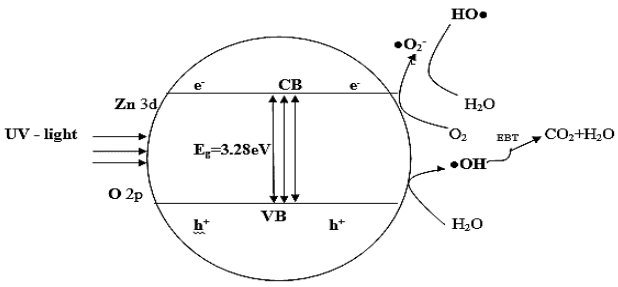

Fig 13. Mechanism of photodegradation of EBT over ZnO nanoparticles

However, in a typical process of photocatalysis, the electrons in valence band (VB) transfer to the conduction band (CB) under UV irradiation of the photocatalyst. The corresponding energy is higher than the band gap of the ZnO (3.28 eV) there by promoting the generation of conduction band electrons and valence band holes. The photogenerated holes could either directly oxidize adsorbed EBT or react with hydroxyl or water to generate hydroxyl radical. Similarly, the photoelectrons reduce oxygen adsorbed on the photocatalyst surface into superoxide radical. Finally, EBT was decomposed by generated hydroxyl and superoxide radical according to the equations 9, 10 and 11.

$$ZnO + h\vartheta \rightarrow h^+ + e^- \quad (9)$$

$$h^+ + OH^- \text{ or } H_2O \rightarrow \bullet OH \quad (10)$$

$$e^- + O_2 \rightarrow \bullet O_2^- \quad (11)$$

To explain fully the mechanism of ZnO nanoparticle for the removal of eriochrome black t, it is very important to determine which reactive species plays a major role in the photocatalytic degradation process. During the photocatalytic removal of EBT over ZnO nanoparticle, the h^+, $\bullet OH$, and $\bullet O_2^-$ are eliminated by adding AO (h^+ scavenger) [33], *t*-BuOH ($\bullet OH$ scavenger) [34] and *p*-BQ ($\bullet O_2^-$ scavenger) [35] into the reaction solution respectively and the result is presented in Fig 14.

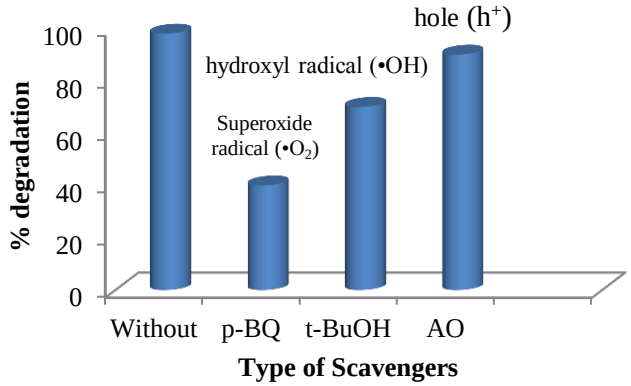

Fig 14. Degradation efficiency of EBT in the absence and presence of scavengers

Fig 14 shows that the addition of *t*-BuOH and AO only slightly changed in the photocatalytic removal of EBT was observed while the addition of *p*-BQ scavenger significantly changed was obtained. These indicate that the decrease of the photocatalytic removal in the presence of scavengers present the following trends: benzo-quinonine > tertiary-butanol > ammonium oxolate, which is very similar to the results of Huang *et al* [36], and Chen *et al* [21]. Hence, the superoxide radicals is the main reactive species during the photocatalytic removal of EBT under UV irradiation.

3.6. Box Behnken Experimental Design and Statistical Analysis

A total of 17 runs of Box-Benhken design were conducted. The EBT degradation efficiencies of the various photoexperiments ($\%D_{exp}$) and statistically predicted (($\%D_{pred}$) are presented in Table 4. The Operating variables in the table are shown in both actual levels.

Table 4: Box benhken design (BBD) with experimental and predicted values

Run	Initial MB concentration (mg/L) (X)	Catalyst loading (gL^{-1}) (Y)	Initial pH (Z)	Experimental efficiency (%)	Predicted efficiency (%)
1	15.00	0.80	12.0	94.35	93.81
2	15.00	0.80	3.00	95.11	95.80
3	15.00	0.40	9.00	96.11	95.95
4	25.00	0.80	9.00	95.32	94.98
5	15.00	0.40	9.00	96.56	96.48
6	15.00	0.40	9.00	96.72	96.51
7	15.00	0.10	12.0	95.33	95.11
8	25.00	0.40	12.0	94.11	94.01
9	25.00	0.10	9.00	95.88	95.25
10	10.00	0.40	3.00	95.77	95.72
11	15.00	0.40	9.00	96.78	96.57
12	15.00	0.10	3.00	95.99	95.11
13	10.00	0.80	9.00	93.13	92.88
14	10.00	0.40	12.0	95.88	95.82
15	10.00	0.10	9.00	94.34	94.11
16	25.00	0.40	3.00	95.12	95.10
17	15.00	0.40	9.00	96.77	96.61

As observed from the Table 4, the closeness of the predicted and experimental values is a primary indication of a true model. Similarly, the table showed good correlation between the experimental and predicted photodegradation efficiencies as attested by linear normal plot of residuals (Fig. 15). Majority of the points on the normal probability plot lies roughly on a straight line, so it can be concluded that the estimated effects are the real and differ markedly from noise.

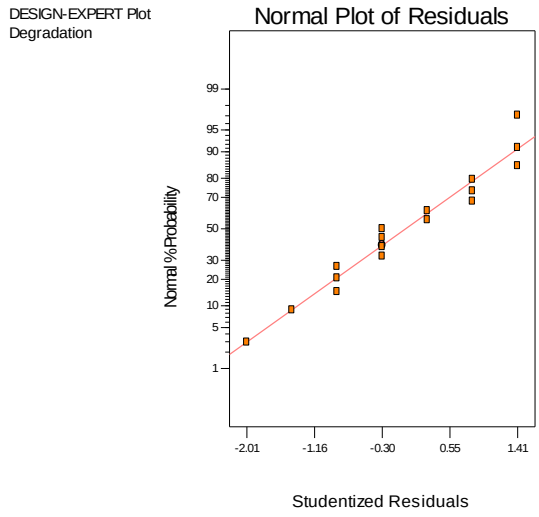

Fig 15. Diagnostic linear normal probability plot of residuals

The optimum photodegradation efficiency of 96.59% was obtained at 15.00mg/L initial concentration of EBT, 0.40g/L catalyst loading and initial pH of 9.00. The relationship between the EBT efficiency (%D) under the influence of EBT initial concentration (X), catalyst concentration (Y) and initial pH (Z) of solution is explained by the quadratic model as given interms of coded and actual factors according to the Eq. 12 and 13 respectively.

$$\%\,D_{pred} = +94.14 + 0.22X + 0.56Y - 0.47Z - 0.83X^2 - 0.46Y^2 + 0.39Z^2 - 0.92XY - 0.58XZ + 0.14YZ \quad (12)$$

and

$$\%\,D_{pred} = 94.13600 + 0.21875\,Conc + 0.56375\,Cataly - 0.46750\,pH - 0.83175\,Conc^2 - 0.45175\,Cataly^2 + 0.38575\,pH^2 - 0.912750\,Conc.Catal - 0.5800\,Conc\,pH + 0.14500\,Cataly\,.pH. \quad (13)$$

The positive sign in front of the terms in Eq. (12 and 13) shows synergistic effect which means improvement in the percent photodegration of eriochrome black t as opposed to the negative sign which shows antagonistic effect [37, 38, 39].

The model quality was obtained by the analysis of variance (ANOVA) and its summary is presented in Table 5. The model F-value of 1265.30 implies that the model is significant and that there is only a 0.01% chance that a model F-value could occur due to some noise. The significance of the model terms is proven by the small p-value less 0.0001. The p-values obtained range from <

0.0001-0.0132 shows that all the model terms are significant. The most significance terms among the tested primary parameters were obtained as EBT concentration > ZnO concentration > second-order of EBT concentration > second-order of ZnO concentration > second-order of solution pH > EBT concentration-solution pH interactions > EBT concentration-ZnO concentration interactions > solution pH > ZnO concentration-solution pH interactions. Therefore, EBT initial concentration (X) and ZnO catalyst dosage (Y) were the most important operating variables that influenced the photocatalyic degradation of EBT over ZnO nanoparticle in comparism with the solution pH (Z), quadratic terms (X^2, Y^2 and Z^2) and interaction terms (XY, XZ and YZ). The ''lack of fit'' (LOF) value is not significant relative to the pure error when f-value is 0.59 and p-value is 0.8398 (more than 0.05) which indicates good predictability of the model.

Table 5: ANOVA for quadratic model.

Source	Sum of Square	DF	Mean Square	F-value	P-value	Comment
Model	167.22	9	14.21	1265.30	< 0.0001	Significant
X	52.42	1	52.42	2821.01	0.0011	Significant
Y	13.11	1	13.11	4324.12	0.0013	Significant
Z	17.38	1	17.38	1324.50	0.0124	Significant
X^2	14.39	1	14.39	311.12	0.0015	Significant
Y^2	1.06	1	1.06	1144.35	0.0043	Significant
Z^2	13.74	1	13.74	3241.22	0.0054	Significant
XY	3.96	1	3.96	1143.16	0.0111	Significant
XZ	1.89	1	1.89	231..28	0.0072	Significant
YZ	0.91	1	0.91	34.15	0.0132	Significant
Residual	215.10	10	215.10			
Lack of fit	121.34	5	120.29	0.59	0.8398	Not significant
Pure Error	0.052	5	49.70			
Total Cor	169.18	19				

However, the standard deviation (S.D = 1.50) and coefficient of variance (C.V = 1.11) (Table 6) are low demonstrated high precision and good reliability of the experimental values. Adequate precision measure of 30.82 which is above 4 shows an adequate signal. The regression model explained a good relationship between independent variables as coefficient of determination R^2 (0.9658) and predicted R^2_{pred} (0.9532) are closed to one. Because of the above mentioned, the quality of the model developed is high and this implies 96% of the variations for the removal of eriochrome blact t were detected by the operating parameters within the studied range. Therefore, the above analysis of variance (ANOVA) shows that this predicted quadratic model is in good consistant with the experimental response and it can be adoped.

Table 6: Analysis of variance (ANOVA) results for the response quadratic

Parameter	Value
Standard deviation (S D)	1.50
Mean	79
Coefficient of variance (CV,%)	1.11
Coefficient of determination (R^2)	0.9658
Adjusted R^2	0.9532
Predicted R^2	0.7111
Adequate precision	30.82

In order to confirm the quadratic model developed in this research, three runs were individually conducted (Table 7) at low, middle and high conditions of the independence variables selected for this study and compared to the predicted responses (Table 4). The experimental responses were very close to the predicted responses (96.48 %) confirming the reliability of the BBD.

Table 7 Confirmation data of the quadratic model.

Run	Initial MB concentration (mg/L)	Catalyst loading (gL^{-1})	Initial pH	Experimental efficiency (%)	Predicted efficiency (%)
1	10.00	0.10	3.00	87.34 ± 0.42	87.76
2	15.00	0.40	9.00	96.48 ± 0.01	96.49
3	25.00	0.80	12.00	80.99 ± 0.16	80.83

3.7 Respone Surface Analysis

The response surface analysis was carried out and the results is presented in Fig 16. Fig 16 (a) shows the three dimensional (3D) graphs and contours plot of response surface of the ZnO catalyst and initial EBT concentration at constant initial pH. It is evident that the removal percentage increased proportionally with increase of photocatalyst dosage due to enhancement in the generation of hydroxyl radicals. Higher catalyst loading was antagonistic to the degradation process, perhaps due to reduction in catalyst surface area available for light absorption and EBT adsorption. On the other hand, the interaction effect of ZnO loading and initial pH of reaction mixture on the degradation of EBT dye is depicted in Fig 16 (b). From the response surface and contour plot, it can be seen that the degradation efficiency was low at acidic pH value due to the loss of ZnO perhaps, whereas at alkaline medium hydroxyl radicals played a positive role in the removal of EBT as earlier observed in the case of other

organic contaminants. The EBT dye has a pKa value of 6.6 and the pH_{pzc} of ZnO is 9 and thus inter electrostatic attraction is favored.

Lastly, the synergistic effect of EBT initial concentration and initial solution of pH in removing EBT dye is clearly revealed by Fig. 16 (c). However, the degradation efficiency reduced with increasing EBT concentration ascribed to the interception of photon before they reach the surface of the ZnO photocatalyst.

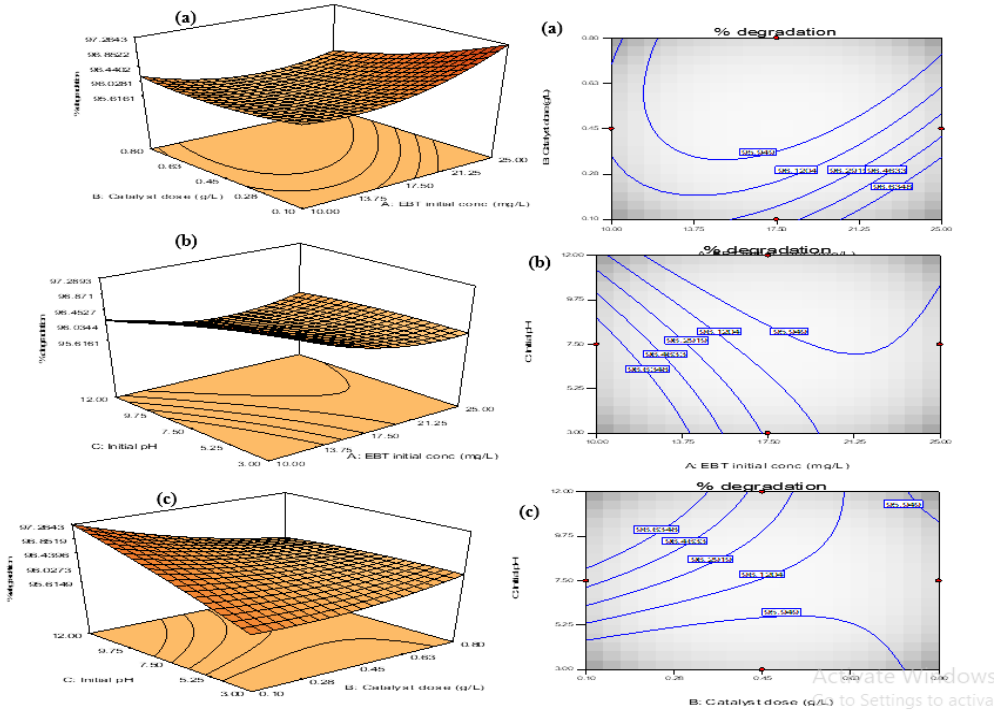

Fig 16. The 3D response surfaces and contour plot for a (a) EBT concentration and ZnO catalyst dosage (b) EBT concentration and initial pH (c) ZnO catalyst dosage and the initial pH.

Moreover, the columbic repulsion between the negatively charged ZnO photocatalyst surface and hydroxyl anions at highly alkaline condition reduced the EBT removal rate via suppression of the generation of hydroxyl radicals.[29]

4. Conclusion

The nanosized ZnO photoresponsive catalyst was successfully synthesized by sol-gel method. The cryatallinity, morphological, elemental and optical properties were obtained by the XRD, SEM, EDS, FT-IR and UV-Visible spectrophotometry. Based on the XRD, SEM and UV-Visible analyses, the synthesized ZnO contain hexagonal wurtzite structure, crystallite size, specific surface area and band gap values were found to be 24.67nm, $36.87 m^2 g^{-1}$ and 3.28eV respectively. It's phototocatalytic performance was evaluated using eriochrome blact t under UV irradiation. The preliminary studies indicated the significant responses. Morever, the reusability and radical scavenging tests on the removal of EBT demonstrated that ZnO photocatalyst is stable for a long period and superoxide ions are the main reactive species. The optimum degradation efficiency of 96.59% was obtained at 15.00mg/L of EBT, 0.40g/L of ZnO catalyst and initial pH of 9.00. Lastly, the degradation model proved that the initial concentration of EBT and ZnO catalyst were the most significant operating variables influencing the degradation of EBT using ZnO nanoparticles.

Acknowledgements

The authors are very grateful to the Department of Applied Chemistry, Faculty of Physical Science Federal University Dutsinma, Katsina state for providing financial supports and most of the facilities required for this research.

.

Conflict of Interest

In this research work there is no conflict of interest

References

1. Robinson T, Kian M, Basil N, Remediation of Dyes in Textiles Effluent: A Critical Review on Current Treatment Technologies with a Proposed Alternative, *Bioresources Technology*. 2001; 77: 247-275.
2. Ezgi A, Mufit B, Mustafa Y, Removal Efficiency of a Calyx [4] Arene-Based Polymer for Water Solible Carcinogenic Direct Azo Dyes and Aromatic Amines. *Journal of Hazard Material*, 2008; 162 (2-3): 960-966.
3. Vaiano V, Matarangolo M, Sacco O, Sannino D, Photocatalytic Removal of Eriochrome Black T Dye over ZnO Nanoparticles doped with Pr, Ce or Eu. *Journal of Chemical Engineering Transctions*. 2017; 57: 625-630.
4. Wang J, Wang Z, Huang B, Ma Y, Liu X, Qin X, Zhang X, Dai Y, Photocatalytic Degradation of Eriochrom Black T Using ZnO Photocatalyst. *Journal of Application Material Interface*. 2012; 4: 4024-4030.
5. Sharma S, Abdullahi B, Ahmad A, Asar B, Photocatalytic Degradation of Eriochrome Back T Using Ammonium Phosphomolybdate Semicomductor as Catalyst Under Visible Light Irradiation .*International Journal of Chemical Engineering*. 2016; 42(1): 31-35.
6. Dunnil A, Van I, Priya A, Xia Q, Ozaki N, Photocatalytic Degradation of Eriochrome Black T Using C-doped TiO_2 Photocatalyst Via Substitutional and Intestitial Dopig. *Journal of Physical Chemistry*. 2018; 37(1):123-129.
7. Bedoui A, Ahmadi MF, Bensalah N Gadri A, Comparative Study of Eriochrome Black T Treatment by BBD Anodic Oxidation and Fenton Process. *Journal of Chemical Engineerig*. 2009; 16:98-109.
8. Priya A, Benz X, Xu Q, Zhai Q, Photocatalytic Degradation of Eriochrome Black T Using Pure and N-doped ZnO Nanoparticles Prepared by Precipitation Method. *International Journal of Applied Chemistry, RSC*. 2015; 31(3): 121-124.
9. Aouni A, Fersi C, Cuartas -Uribe B, Bes-Pia A, Alcaina-Miranda M I, Dhabi M, Reactive Dyes Rejection and Tertile Effluent Treatment Study Using Ultrafiltration and Nanofiltration Processes. *Desalination*. 2012; 297:87-96.
10. Gaya U I, Heterogeneous Photocatalysis Using Inorganic Semiconductor Solids. *Springer*. 2014; Dordrech: 2-14
11. Hamza A, Fatuase J T, Waziri S M, Ajayi O, Solar Photocatalytic Degradtion of Phenol Using ZnO . *Journal of Chemical Engineering*. 2013; 89-90.
12. Vaiano L, Sacco O, Sannino D, Ciambelli O, N-doped ZnO Nanoparticles Supported on ZnS Based Blue Phosphors in the Photocatalytic Removal of Eriochrome Black T. *Journal of Engineering Transactions*. 2016; 23: 232-237.
13. Xu X, Zhang Q P, Ong B T, Yuan H, Chen Y, Liu Y T, Xu M, Influence of Stabilzer on the Microstructrure and Photocatalytic Performance of ZnO Nanopowder Synthesized by Sol – gel Method. *Journal of Nanotechnology*. 2017; 50: 57-71.
14. Lu C,Wu Y, Mai F, Chung F, Wu Lin C, Chen C, Degradation Efficienties and Mechanism of ZnO Mediated Photocatalytic Degradation of Eriochrome Black T under Ultraviolet Light Irradiation. *Journal of Molecular Catalysis*. 2009; 30:159-165.
15. Raoufi D, Synthesis and Microstrucural Properties of ZnO Nanoparticles Prepared by Precipitation Method. *Renewable Energy*. 2013; 5(2): 932-937.
16. Savaranan V K, Gupta V, Narayan A, Comparative Study on Photocatalytic Activity of ZnO Prepared by Different Methods. *Journal of Photochemistry and Photobiology*. 2013; 181:133-141.
17. Sarith A, Shank H, Prakash T, Sampa C, Photocatalytic Degradation of Eriochrome Black T in Aqueous Medium under Ultraviolet and Visible Light Irradiation by TiO_2 and ZnO Nanoparticles. *Journal of Hazardous Material*. 2017; 45(2): 335-340.
18. Supamas S, Schrank S, Josa P, Hiranok YT, Photocatalytic Degradation of Eriochrome Black T Using TiO_2 as photocatalyst. *Journal of Photochemistry and Photobiology*. 2014; 34:225-258.
19. Maureen O O C, Nnaemeke OJ, Basil NA, Emeka EO, Photocatalytic Degradation of a Basic Dye using Zinc Oxide Nanocatalyst. *International Letter of Chemistry, Physis and Astronomy*. 2019; (81): 18-26.
20. Kian M, Lee S, Abdulhamid B, and China W, Multivariate Analysis of Photocatalytic-Mineralization of Eriochrome Black T Dye using ZnO catalyst under UV irradiation. *Journal of Nanotechnology and Catalysis Research Centre*. 2015; 42: 102-112.
21. Chen XW, Danden L, Zhen G, Preparation of ZnO Photocatalyst for the Efficient and Rapid Photocatalytic Degradation of Azo Dyes. *Nanoscale Research Letters*, 2017; 12-13.
22. Yusuf A, Gaya U I, Mechanochemical Synthesis and Characterization of N-doped TiO_2 for Photocatalytic Degradation of Caffeine. *Journal of Nanochemistry*.2018; 3(1): 29-35.
23. Yoshio K, Onodera A, H, Satoh A. H, Sakagami N, and Yamashita H, Crystal Structure of ZnO: Li At 293 K and 19 K by X-ray Diffraction. *Ferroelectr*. 2001; 264(1):133-138.
24. Dodoo-Arhin D, Asiedu T, Agyei-Tuffour B, Nyankson E, Obada D, Mwabora J. M, Photocatalytic Degradation of Rhodamine Dyes Using Zinc Oxide Nanoparticles. *Material Today: Proceeding*. 2021; 38(2): 809-815.
25. Algarni T. S, Abdah N. A. Y, Kahtani A. A and Aoussi, Photocatalytic Degradation of Some Dyes Under Solar Light Irradiation Using ZnO Nanoparticles Synthesized from Rosmarinus Officinalis Extract. *Green Chemistry Letters and Reviews*. 2022; 15(2): 460-473.

26. Kaman T and Selvakumar S. A.S, Biosynthesis of ZnO Nanoparticles Using Rambutan (Nephelium Lappaceum L) Peel Extract and their Photocatalytic Activity on Methyl Orange Dye. *Journal of Molecular Structure*. 2016; 1125: 358-365.
27. Jeevanandam J, Barhoun A, Chan Y. S, Dufresne A, Danguah M. K, Review on Nanoparticles and Nanostructures Materials: History, Sources, Toxicity and Regulations. *Beilstein Journal of Nanotechnology*. 2018; 9(1): 1050-1074.
28. Lanjwani M. F, Muhammad Y, Khuhawar T, Khuhawar J. Lanjwani A, Memon S. Q, Soomro W. A, Rind I. K, Photocatalytic Degradation of Eriochrome Black T Dye By ZnO Nanoparticles Using Multivariant Factorials, Kinetics and Isotherm Model. *Journal of Cluster Science*. 2022; 23: 293-8.
29. Fakhari S, Jamzad M, Fard H. K, Green Synthesis of Zinc Oxide Nanoparticles: a Comparison. *Green Chemistry Letters and Reviews*. 2019; 12(1): 19-24.
30. Shah S. N, Ali S. I, Ali S. R, Neem M, Bibi Y, Ali S. Raza S. M, Khan Y, and Sherwani S. K, Synthesis and Characterization of Zinc Oxide Nanoparticles for Antibacterial Applications. *Journal of Basic and Applied Sciences*. 2016; 12: 205-210.
31. Saravanann R, Shankar H, Rajasudha G, and Stephen A, Photocatalytic Degradation of Organic Dye By Nano ZnO. *International Journal of Nanoscience*. 2011; 10(1): 253-257.
32. Suresh P, Michael S, Nicholas N, Miguel G, Athanassion K, Mohammad HE, Patrick SM, Jeremy WJ, Anthony B, Kevin O, Dionysios DD, A Review on the Visible Light Active ZnO Photocatalysts for Environmental Applications. *Chemosphere*. 2012; 125:331-349.
33. Akhund A, Habibi-Yangjeh A, Ternaary Magnetic g-C_3N_4/Fe_3O_4/AgI Nanocomposites: Novel Recyclable Photocatalysts with Enhanced Activity in Degradation of Different Pollutants under Visible Light. *Material Chemical Physics*. 2016; 174: 59-69.
34. Shellofteh-Gohari M, Habibi-Yangjeh A, Novel Magnetically Separable Fe_3O_4@ZnO/AgCl Nanocomposites with Highly Enhanced Photocatalytic Activities under Visible Light Irradiation. *Sep Purifi Technol*. 2015; 147: 194-202.
35. Wang J, Jiang WJ, Liu D, Wei Z, Zhu YF, Photocatalytic Performance Enhanced via Surface Bismuth Vacancy of $Bi_6S_2O_{15}$ Core/Shell Nanowires. *Applied Catalysis of B Environment*. 2015; 176: 306-314.
36. Huang N, Shu JX, Wang ZH, Chen M, Ren CG, Zhang W, One Step Pyrolytic Synthesis of ZnO Nanorods with Enhanced Photocatalytic Activity and High Photostability under Visible and UV Light Irradiation. *Journal of Alloys Compounds*. 2015; 648: 919-929.
37. Jurex A, Zheng X, Zhai Z, Zhao Q, Optimizaton for Photocatalytic Degradation of Eriochrome Black T Using Immobilized Ac/TiO_2. *Journal of Photochemistry and Photobiology, RSC*. 2012; 31(2): 111-118.
38. Zhang J, Fu D, Xu Y, Liu C, Optimization of Parameters on Photocatalytic Degradation of Chloramphenicol Using TiO_2 as Photocatalyst by Response Surface Methodology. *Journal of Hazardous Environmental Science*. 2010; 22: 1281-1289.
39. Zarei M, Niaei A, Salari D, Khataee A, Application of Response Surface Methodology for Optimization of Peroxi Coagulation of Textile Dye Solution Using Carbon Nanotube PTFE Cathode. *Journal of Hazardous Materials*. 2010; 173: 544-551.

Recommended Citation

Yusha'u A, Darma MS, Isah KB. Sol-gel Synthesis of ZnO nanoparticles for optimized photocatalytic degradation of Eriochrome Black T under UV irradiation. *Alger. J. Eng. Technol. 2023*; 8(1): 117-130. DOI: https://doi.org/10.57056/ajet.v8i1.100